

Left-handed W bosons at the LHC

Z. Bern,¹ G. Diana,² L. J. Dixon,^{3,4} F. Febres Cordero,⁵ D. Forde,^{3,6} T. Gleisberg,⁴
S. Höche,⁴ H. Ita,¹ D. A. Kosower,² D. Maître,^{3,7} and K. Ozeren¹

¹*Department of Physics and Astronomy, UCLA, Los Angeles, California 90095-1547, USA*

²*Institut de Physique Théorique, CEA-Saclay, F-91191 Gif-sur-Yvette cedex, France*

³*Theory Division, Physics Department, CERN, CH-1211 Geneva 23, Switzerland*

⁴*SLAC National Accelerator Laboratory, Stanford University, Stanford, California 94309, USA*

⁵*Universidad Simón Bolívar, Departamento de Física, Caracas 1080A, Venezuela*

⁶*NIKHEF Theory Group, Science Park 105, NL-1098 XG Amsterdam, The Netherlands*

⁷*Department of Physics, University of Durham, Durham, DH1 3LE, United Kingdom*

(Received 24 April 2011; published 5 August 2011)

The production of W bosons in association with jets is an important background to new physics at the LHC. Events in which the W carries large transverse momentum and decays leptonically lead to large missing energy and are of particular importance. We show that the left-handed nature of the W coupling, combined with valence quark domination at a pp machine, leads to a large left-handed polarization for both W^+ and W^- bosons at large transverse momenta. The polarization fractions are very stable with respect to QCD corrections. The leptonic decay of the W^\pm bosons translates the common left-handed polarization into a strong asymmetry in transverse momentum distributions between positrons and electrons and between neutrinos and antineutrinos (missing transverse energy). Such asymmetries may provide an effective experimental handle on separating W + jets from top-quark production, which exhibits very little asymmetry due to C invariance, and from various types of new physics.

DOI: [10.1103/PhysRevD.84.034008](https://doi.org/10.1103/PhysRevD.84.034008)

PACS numbers: 13.88.+e, 12.38.Bx, 13.38.Be, 14.70.Fm

I. INTRODUCTION

Events produced by new physics at the LHC often resemble events generated by standard-model physics. This is especially true for signals involving multiple jets alongside a W boson that decays to a lepton pair. These kinds of events most commonly arise from QCD emission in an electroweak process. Such events could also be the result of cascade decays in supersymmetric extensions of the standard model, as well as in other models of physics beyond the standard model. They also emerge in top-quark pair production in its semileptonic decay mode and in some Higgs search modes. The QCD W + jets events pose a background to all of these signals.

The superficial similarity of such signals to overwhelmingly larger backgrounds pushes us to find differences in various distributions, so as to impose cuts that suppress the standard-model backgrounds while retaining as much of the signals of new physics as possible. General underlying properties or principles that distinguish different sources of similar events are of particular importance. In this paper, we discuss one such general property, the large left-handed polarization of high- p_T “prompt” W^+ and W^- vector bosons produced directly in short-distance standard-model interactions [1]. This effect is distinct from the well-known [2] left-handed polarization of low- p_T W bosons moving primarily along the beam axis.

The importance of W + n -jet final states in hadron-collider searches has prompted intensive theoretical work over the last two decades. Leading-order (LO) matrix-element generators have been available for some time

[3,4]. More recently, they have been combined with parton-shower approaches using several matching techniques [5], in order to provide event simulations which combine the correct wide-angle properties (at LO) with the detailed intrajet particle distributions required by experimenters. LO predictions, however, leave the overall normalization of event rates uncertain, an uncertainty that rises as the number of jets increases.

Obtaining quantitatively reliable predictions for W + n -jet rates and distributions requires next-to-leading order (NLO) cross sections in QCD. The one-loop matrix elements entering NLO predictions stabilize the dependence on the unphysical renormalization and factorization scales and provide predictions expected to be reliable to 10%–15%. Until recently, calculating the required one-loop matrix elements posed a major difficulty, especially for final states with many jets (and hence many partons). Unitarity-based techniques have broken this bottleneck, and have allowed the prediction at NLO of vector-boson production with up to four associated jets [1,6–9]. These predictions do indeed possess greatly reduced overall normalization uncertainties. They also indicate where the LO predictions for shapes of distributions are reliable and where they suffer corrections. For more than one associated jet, the results are available at the parton level and have not yet been incorporated into a matched parton shower maintaining NLO accuracy.

It was first observed in Ref. [1] that for W + 1, 2, 3-jet events at the LHC, both W^+ and W^- bosons produced via standard-model interactions are preferentially polarized

left handed along their flight direction, beyond small transverse momenta. The polarization manifests itself in the decay spectra of the daughter leptons: left-handed W^+ bosons at a fixed boson p_T^W produce larger neutrino transverse momentum (missing E_T) and smaller charged lepton p_T , in comparison with the decays of left-handed W^- bosons. The polarization thus gives a characteristic shape to the ratios of the charged-lepton E_T spectra, as shown in Fig. 1, between W^+ and W^- production in association with three jets. (The precise setup used for this plot may be found in Ref. [1]; the key feature, a falling ratio with increasing E_T , is generic.) An opposite but similarly characteristic shape arises in the ratio of missing E_T distributions for W^+ versus W^- events. These ratio distributions are quite stable upon going from LO to NLO. Ref. [10] computed directly the left, right and longitudinal polarization fractions f_L , f_R and f_0 for the case of $W^+ + 2$ -jet production at the LHC. The polarization fractions are quite stable over a range of W transverse momenta, with f_L of order 60% and rising slowly with p_T^W , f_R of order 25%, and the remaining longitudinal fraction f_0 dropping monotonically toward zero as p_T^W increases. The vanishing of f_0 at large p_T^W is dictated by the equivalence theorem [11] because the Goldstone modes cannot couple to light quark lines.

In this paper we explore the dynamics behind the production of left-handed prompt W bosons at finite transverse momentum at the LHC. We explain the underlying mechanism in terms of a combination of the left-handed nature of the charged-current weak interactions (which allows only left-handed quarks to participate at lowest order), the domination of quarks over antiquarks in the incoming protons, and the structure of the relevant helicity amplitudes.

Our earlier results [1,10] have prompted CMS to undertake a measurement of W boson polarization using the 2010 LHC data collected at $\sqrt{s} = 7$ TeV [12]. Here we provide theoretical predictions relevant to this measurement, which require a minimum p_T^W of 50 GeV but no explicit requirement of additional jets. We apply no

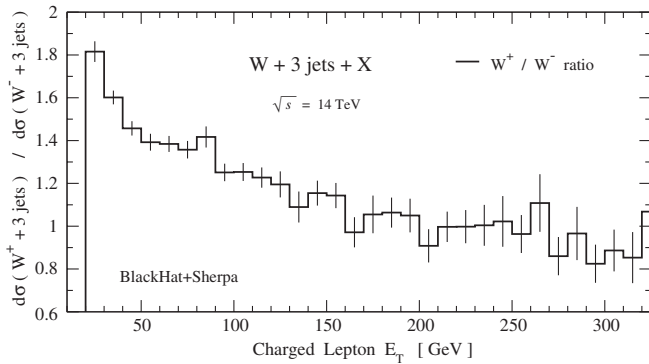


FIG. 1. The ratio of the charged-lepton E_T distributions at the LHC for W^+ and W^- production in association with three jets, evaluated at NLO [1].

explicit cuts on the lepton transverse momenta or rapidity and no lepton isolation cuts either. The experiments do, of course, make such cuts—the detectors have finite size and cracks, and triggers impose implicit lepton p_T cuts. CMS has corrected its measured data for the effects of the lepton cuts. The actual cuts used, combined with the lack of knowledge of the longitudinal component of the neutrino momentum, lead to a dependence of the extracted fractions f_L , f_R , and f_0 on other components of the full W boson spin density matrix.

The diagonal elements of the density matrix (essentially f_L , f_R , and f_0) are coefficients of functions that depend only on the polar angle θ^* of the charged lepton in the W rest frame, with respect to the W flight direction as observed in the lab frame. The neutrino will of course come out at an angle $\pi - \theta^*$ in this frame. The off-diagonal elements arise from the interference of amplitudes for different W helicity states, and they depend on an azimuthal angle ϕ^* . They would integrate to zero if the experimental acceptance were uniform in ϕ^* , but it is not. Accordingly, theoretical information about the ϕ^* dependence, and its uncertainty, is needed in order to extract f_L , f_R , and f_0 . The full W spin density matrix has been studied previously in several theoretical papers [13–18]. Two of the additional coefficients were measured by CDF during Run I of the Tevatron [19].

In this paper we compute the diagonal and off-diagonal elements of the density matrix as a function of the W boson transverse momentum at the LHC at $\sqrt{s} = 7$ TeV, expressed as asymmetry coefficients A_i of various angular distributions. We perform the computation at LO and at NLO, i.e. fixed-order and parton level, using BLACKHAT [20] in conjunction with SHERPA [21]. We also use SHERPA to provide a parton-shower prediction matched to tree-level matrix elements, also known as matrix-element-plus-truncated-shower (ME+PS). (Our parton-shower results do not include hadronization effects but remain at the parton level.) We find that the corrections from LO to NLO are fairly small. We also find that varying the factorization and renormalization scale in a correlated way in the numerator and denominator of the ratios entering the A_i gives very small changes, so small that it does not provide a sensible measure of the theoretical uncertainty. We have studied the dependence of the A_i on the parton distributions, using the error sets provided by CTEQ [22], and find it to be small as well.

We ascribe the principal theoretical uncertainty to the difference between the NLO and ME+PS results. This difference is typically of order 10% for the larger A_i coefficients, including f_L , f_R , and f_0 . (The uncertainties from the choice of parton distributions are significantly smaller.) Some of the A_i coefficients are quite small in magnitude, presumably due to cancellations between different types of terms. In this case the percentage difference between NLO and ME+PS can be significantly larger.

This article is organized as follows. In Sec. II we give arguments why W bosons are predominantly left handed at the LHC. In Sec. III we define the polarization more precisely and explain how we compute it. Our results are presented in Sec. IV. In Sec. V we give our conclusions.

II. DYNAMICS OF W POLARIZATION AT THE LHC

In this section we will explain why both W^+ and W^- bosons produced at the LHC are dominantly polarized left handed when they emerge with large transverse momentum. We will start with a heuristic explanation based on angular momentum conservation and then proceed to refine the explanation further. A fully quantitative description requires a numerical calculation, which we present in Sec. IV.

Before considering the case of W production with transverse momentum, we discuss the simpler and well-known example of W polarization along the beam axis for W bosons produced with little or no transverse momentum [2]. Here the principal production mechanism involves the leading-order partonic subprocesses $u\bar{d} \rightarrow W^+$ and $d\bar{u} \rightarrow W^-$. At leading order, the W moves strictly along the beam axis, with no transverse momentum, $p_T^W = 0$. Suppose the W is moving in the direction of the initial-state quark, as opposed to the antiquark. This is likely to be the case at the LHC, because the LHC is a pp machine and the quark distributions $q(x)$ have a larger average momentum fraction x than the antiquark distributions $\bar{q}(x)$. Because the electroweak charged current is purely left handed, the quark must be left handed and the antiquark right handed. (We assume massless quarks and leptons throughout this paper.) By angular momentum conservation, the spin of the W is 100% left handed along its direction of motion, for either W^+ or W^- , as shown in Fig. 2. This effect is diluted some by antiquarks that occasionally carry a larger x than the quarks with which they collide. However, the dilution is small at large rapidities because the ratio $q(x)/\bar{q}(x)$ increases rapidly as $x \rightarrow 1$.

The W polarization is analyzed with 100% analyzing power through its leptonic decay. A left-handed W^+ tends to decay with the left-handed neutrino forward (along its direction of motion) and the right-handed positron backward. A left-handed W^- tends to put the left-handed

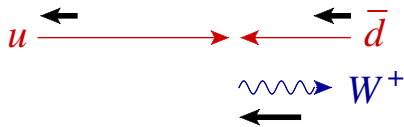


FIG. 2 (color online). When a W^+ is produced at lowest order by $u(x_1)\bar{d}(x_2) \rightarrow W^+$ with $x_1 > x_2$, it is 100% left-handed polarized along its direction of motion, which is along the beam axis in the quark direction. Thick (black) arrows represent spin vectors; the other arrows represent momentum vectors in the pp center-of-mass frame.

electron forward and the right-handed antineutrino backward.

Note that at the Tevatron, a $p\bar{p}$ collider, the same basic physics of valence quark domination and angular momentum conservation, causes the W^+ bosons, which typically move in the proton direction, to be primarily left handed. However, the W^- bosons, which typically move in the antiproton direction, usually arise from a right-handed \bar{u} antiquark from the antiproton annihilating with a left-handed d quark from the proton; hence the W^- bosons are predominantly right handed at the Tevatron. This polarization implies that both W^+ and W^- bosons tend to decay so that the charged leptons are more central than the parent bosons, producing the well-known dilution of the W boson charge asymmetry, when it is measured via the charged-lepton rapidity distribution.

Next consider the case in which the W boson does carry transverse momentum. For definiteness, we take the W to be a W^+ ; the case of a W^- is qualitatively the same. At leading order, there are three possible subprocesses: $ug \rightarrow W^+d$, $u\bar{d} \rightarrow W^+g$, and $g\bar{d} \rightarrow W^+\bar{u}$. These subprocesses are all related to each other by crossing symmetry. For events with a sufficiently large W transverse momentum, the soft-gluon enhancement of $u\bar{d} \rightarrow W^+g$ is not that important, and the hierarchy of subprocess contributions is set by the hierarchy of relevant parton distributions for typical values of x . Now, x increases with p_T^W ; at sufficiently large x , $q(x) \gg g(x) \gg \bar{q}(x)$, which leads to the subprocess hierarchy,

$$\frac{d\sigma(ug \rightarrow W^+d)}{dp_T^W} > \frac{d\sigma(u\bar{d} \rightarrow W^+g)}{dp_T^W} > \frac{d\sigma(g\bar{d} \rightarrow W^+\bar{u})}{dp_T^W}, \quad (2.1)$$

once we include the convolution with parton distributions in the quantities in Eq. (2.1). Even at more moderate p_T^W (smaller x), where the second hierarchy might be small, or even reversed, the first one should still hold. (Kom and Stirling [23] have found that at LO the fraction of subprocesses in $W + 1, 2, 3, 4$ -jet production that are initiated by the qg channel (plus $\bar{q}g$) is around 70%–80%.)

Consider the W polarization produced by the dominant subprocess, $ug \rightarrow W^+d$. The analysis is more complicated than in the case of production along the beam axis because two different axes are involved, the beam line and the W flight direction. In this section only, to simplify the analysis we define the W flight direction using the partonic center-of-mass frame. (In subsequent sections we will use the lab frame; at very high p_T^W there is not much difference between these choices.) There are two Feynman graphs for this process, shown in Fig. 3, the s -channel graph on the left and the t -channel graph on the right. We first give an heuristic argument that the W is left handed, based on angular momentum conservation along the W flight direction.¹ Suppose for a moment that we could neglect the

¹We thank Jeff Richman for suggesting this argument.

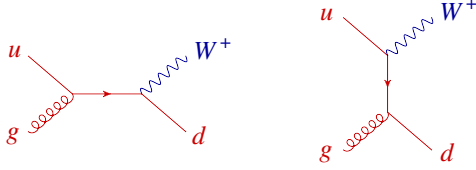


FIG. 3 (color online). The two Feynman graphs for the subprocess $ug \rightarrow W^+d$.

t -channel graph. Then the subprocess would involve an off-shell spin-1/2 u quark, which decays to an on-shell, left-handed d quark recoiling against the W boson. In this case it is impossible for the W boson to be right handed because the total angular momentum along the W - d axis would then be $1 + 1/2 = 3/2$, which cannot be carried by the spin-1/2 off-shell quark. Also, the longitudinal mode of the W is suppressed for large transverse momenta, $p_T^W \gg M_W$, by the equivalence theorem which relates this mode to the Goldstone boson, which does not couple to massless fermions. Thus we could argue that the W boson is 100% left handed at large p_T^W if only we could neglect the t -channel graph.

In fact, this argument is true when the incoming gluon is left handed. To see this, we choose the gluon polarization vector so that the t -channel graph in Fig. 3 vanishes. This graph contains a factor of $\varepsilon^\pm(k_g, q)|k_d^+\rangle$, where $|k_d^+\rangle$ is a Weyl spinor for the outgoing d quark momentum k_d , and $\varepsilon_\mu^\pm(k_g, q)$ is the polarization vector for the gluon with momentum k_g . We use a spinor-helicity representation for this polarization vector, in terms of a reference momentum/spinor q . Contracting with γ^μ yields the gluon polarization bi-spinors,

$$\varepsilon^+(k_g, q) = \frac{\sqrt{2}|k_g^-\rangle\langle q^-|}{\langle qk_g\rangle}, \quad (2.2)$$

$$\varepsilon^-(k_g, q) = -\frac{\sqrt{2}|q^-\rangle\langle k_g^-|}{[qk_g]}, \quad (2.3)$$

using a standard all-outgoing labeling of the gluon helicity \pm , where we dropped terms that vanish when contracted with a left-handed d or u spinor. For a left-handed incoming gluon, as shown in Fig. 4(a), we are instructed to use Eq. (2.2). In this case the t -channel graph is proportional to $\langle q^-|k_d^+\rangle \equiv \langle qk_d\rangle$. We are now free to choose the reference spinor $q = k_d$, so that $\langle qk_d\rangle = 0$ and thus the t -channel graph vanishes. Although this is a specific gauge choice, it allows us to argue that the W should be 100% left handed when the incoming gluon is left handed, at least at very large p_T^W , and when the W spin is analyzed along the W flight direction, as measured in the partonic center-of-mass frame. We will see in a moment that this statement is true even at lower p_T^W . The purely left-handed W polarization is indicated by a long downward-pointing vertical arrow next to the W in Fig. 4(a).

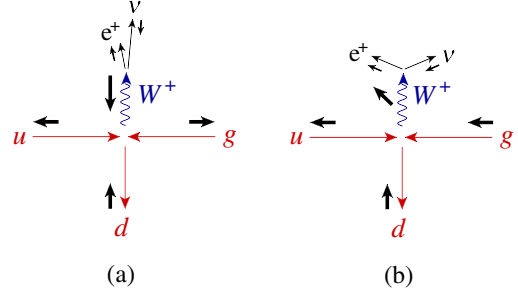


FIG. 4 (color online). Helicity configurations for the subprocess $ug \rightarrow Wd$ for (a) a left-handed incoming gluon and (b) a right-handed one. Thick arrows again denote spin vectors. In case (a) the W is purely left handed, after boosting from the partonic center-of-mass frame. In case (b) it has indefinite polarization but becomes purely right handed at large W transverse momentum, as indicated by the arrow at an angle. However, the squared matrix element is smaller than in case (a).

In contrast, when the incoming gluon is right handed, as in Fig. 4(b), we use Eq. (2.3) for the gluon polarization bi-spinor. Now $|q^-\rangle$ enters a more complicated spinor string, and we cannot make the t -channel graph vanish by a simple choice of q . (We could make the s -channel graph vanish if we wanted to, but that would not help in an angular-momentum-based argument.) In accordance with this obstruction, the outgoing W now can have any of the three possible helicities. We will see shortly that when the W transverse momentum becomes large, its polarization is dominantly right handed. The indefinite W polarization, but transitioning to right handed, is indicated by a short arrow angling upward, next to the W in Fig. 4(b).

The reason the right-handed W polarization in case (b) does not wash out the left-handed polarization in case (a) at large transverse momenta is because the magnitude of its squared matrix element is only about 1/4 the size of the one in case (a). This smaller weighting leads to an estimated asymptotic polarization, at very large W transverse momentum, of roughly 80% left handed and 20% right handed. In this limit, the left-handed W bosons all come from left-handed gluons, and the right-handed ones are all from right-handed gluons. We will see later in the paper that the actual W polarizations predicted, at transverse momenta accessible at the LHC, are remarkably close to this asymptotic value.

The leading-order amplitudes for the three subprocesses in Eq. (2.1) are all related by crossing symmetry. After decaying the W to a lepton pair, $W^+ \rightarrow l^+\nu$, they can all be written simply in terms of spinor products,

$$\mathcal{A}_{(a)}^{\text{tree}} \propto \frac{\langle d\nu\rangle^2}{\langle ug\rangle\langle gd\rangle} \Rightarrow d\sigma_{(a)}^{\text{LO}} \propto (k_d \cdot k_\nu)^2, \quad (2.4)$$

$$\mathcal{A}_{(b)}^{\text{tree}} \propto \frac{[ue]^2}{[ug][gd]} \Rightarrow d\sigma_{(b)}^{\text{LO}} \propto (k_u \cdot k_e)^2, \quad (2.5)$$

where we dropped coupling and propagator factors common to the two cases. The helicity configurations (a), given by Eq. (2.4), are depicted in Figs. 4(a), 5(a), and 6(a). The configurations (b), given by Eq. (2.5), are shown in Figs. 4(b), 5(b), and 6(b).

For Fig. 4(a), the factor of $(k_d \cdot k_\nu)^2$ in the W rest frame is proportional to $(1 - \cos\tilde{\theta}^*)^2$, where $\tilde{\theta}^*$ is the angle between the charged lepton and the W flight direction, as measured in the partonic center-of-mass frame. This is also the angle between the d quark and neutrino directions. This angular dependence implies the purely left-handed W boson polarization mentioned above. In contrast, for Fig. 4(b), the factor of $(k_u \cdot k_e)^2$ does not lead to a net left-handed polarization. It correlates the positron direction with the incoming beam direction rather than with the outgoing W flight direction. In the limit of large transverse momentum, when one boosts from the parton center-of-mass frame to the W rest frame, the incoming u quark and gluon are almost parallel, and their spatial momentum adds up to give the outgoing d quark momentum. If the scattering angle is 90° in the center-of-mass frame, then the magnitude of the u quark momentum is precisely half that of the d quark, in the W rest frame. Then the numerator factor $(k_u \cdot k_e)^2$ in Eq. (2.5) yields the opposite polarization from $(k_d \cdot k_\nu)^2$ in Eq. (2.4) but only at $1/4$ the rate, i.e. it is proportional to $\frac{1}{4}(1 + \cos\tilde{\theta}^*)^2$.

A partonic scattering angle of 90° kinematically maximizes p_T^W at fixed parton center-of-mass energy, i.e. at fixed $x_1 x_2$ for $u(x_1)g(x_2) \rightarrow W^+ d$. However, the matrix element prefers a smaller scattering angle (the d quark more parallel to the incoming gluon), while the parton densities prefer $x_1 > x_2$, which further skews the preferred kinematics. Hence the 80% value for f_L that is implied by 90° scattering is just an estimate for asymptotically large p_T^W .

At finite W transverse momentum, we find that the polarization fractions for 90° $ug \rightarrow Wd$ scattering in case (b) are

$$f_L = \frac{1}{4}(1 - \cos\theta_u)^2, \quad f_R = \frac{1}{4}(1 + \cos\theta_u)^2, \quad (2.6)$$

$$f_0 = \frac{1}{2}\sin^2\theta_u,$$

where θ_u is the angle that the u quark makes with the d quark in the W rest frame. In terms of the boost of the W boson in the partonic center-of-mass frame, $\gamma = E_W/M_W$, it satisfies

$$\sin\theta_u = \frac{1}{\gamma}. \quad (2.7)$$

At 90° , the overall weighting of this helicity configuration, with respect to case (a), is $1/(4\cos^2\theta_u)$. From these relations one can estimate the LO polarization fractions from this subprocess at finite p_T^W .

The subprocess $u\bar{d} \rightarrow W^+ g$ shown in Fig. 5 is subdominant to $ug \rightarrow W^+ d$, but it can be analyzed similarly using

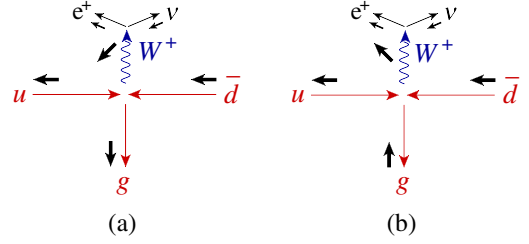


FIG. 5 (color online). Helicity configurations for the subprocess $u\bar{d} \rightarrow Wg$ for (a) a right-handed outgoing gluon and (b) a left-handed one. The directions of the W spin arrows are discussed in the text.

Eqs. (2.4) and (2.5). In both cases the decay leptons are correlated with the beam direction. At large W transverse momenta, case (a) yields mainly left-handed W bosons, while (b) yields mainly right-handed ones (as indicated by the arrows next to the W 's in the figure). For 90° scattering, the two cases for $u\bar{d} \rightarrow W^+ g$ cancel, and there is no net left-handed polarization from this subprocess. Finally, the subprocess $g\bar{d} \rightarrow W^+ \bar{u}$ is shown in Fig. 5. It produces a net right-handed W polarization, from configuration (b), because the factor $(k_u \cdot k_e)^2$ is proportional to $(1 + \cos\tilde{\theta}^*)^2$. However, it is suppressed compared to the dominant source of left-handed polarization in Fig. 4(a) because $u(x) \gg \bar{d}(x)$ except at quite small x .

We have argued that the W polarization should reach about 80% left handed and 20% right handed at asymptotically large W transverse momentum. However, there are a number of reasons why the left-handed fraction should be smaller at finite p_T^W :

- (1) The mainly right-handed configuration in Fig. 4(b) competes better against the pure left-handed one in Fig. 4(a) for smaller p_T^W .
- (2) The 100% left-handed fraction found in Fig. 4(a) was analyzed with respect to a W flight direction measured from the partonic center-of-mass frame, but the conventional definition is from the pp center-of-mass frame, which differs whenever the u quark and gluon momentum fractions are not identical.
- (3) The subdominant $u\bar{d}$ and $g\bar{d}$ channels dilute the polarization. The dilution decreases as x increases, i.e. as p_T^W increases (or as other measures of the hardness of the event increase, such as the scalar transverse energy H_T for a W + multi-jet event).
- (4) While QCD corrections are generally expected to be small—and we will confirm this expectation in this paper—in principle they can affect the W polarization fractions.

Note that the third remark suggests that the left-handed fraction for W^+ bosons should be a bit larger than the left-handed fraction for W^- bosons, at a given p_T^W . This property should hold because in the proton $u(x) > d(x)$, which

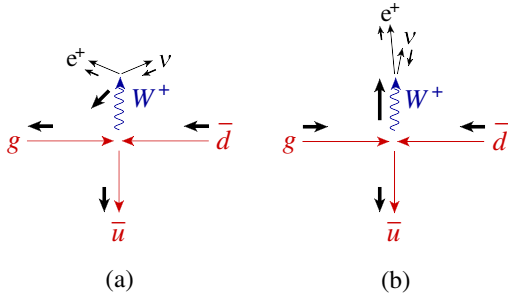


FIG. 6 (color online). Helicity configurations for the subprocess $g\bar{d} \rightarrow W\bar{u}$ for (a) a left-handed incoming gluon and (b) a right-handed one. Case (b) yields a purely right-handed W boson, while case (a) tends toward left handed at large p_T^W but with a smaller weight, as indicated by the arrow.

allows the dominance of $ug \rightarrow W^+d$ over $g\bar{d} \rightarrow W^+\bar{u}$ to set in before that of $dg \rightarrow W^-u$ over $g\bar{u} \rightarrow W^-\bar{d}$.

In Refs. [1,10], left-handed W polarization effects were shown to be large in $W + 2$ -jet and $W + 3$ -jet production for moderate to large p_T^W . The generic kinematics for these processes are quite complicated, and we do not fully understand why the polarization is so large here. For very large W transverse momentum, the configuration preferred by the fast-falling parton distributions is one in which the W recoils against a cluster of jets with relatively small invariant mass. In this limit, the multiparton amplitudes can be factorized [1] into the ones for a W recoiling against a single parton, multiplied by collinear or multicollinear QCD splitting amplitudes. Because the QCD splitting amplitudes are invariant under parity, one can use the same argument given above for the case of $W^+ + 1$ -jet production (or alternatively, for W production at a finite transverse momentum, with no explicit jet requirement). However, for moderate W transverse momenta, close to the jet p_T threshold, the configuration in which a W boson recoils against a small invariant-mass cluster of jets should be fairly rare, and so this argument would not apply.

In any case, it is not difficult to confirm using standard Monte Carlo programs that the average degree of polarization at large p_T^W is rather insensitive to the number of jets. In Fig. 7 we compare the polarization fractions as a function of p_T^W for $W^+ + 1, 2, 3$ -jet production at (unshowered, fixed-order) LO, using the SHERPA package. For these plots we imposed a $p_T > 30$ GeV cut on the jets, using the SISCONT jet algorithm [24] with $R = 0.4$ and the CTEQ6L1 [22] parton distribution set. Beyond low vector-boson p_T , the three cases are remarkably similar, with f_L reaching 70% at high vector-boson p_T . (The sharp cutoff of events below 30 GeV for the $W + 1$ -jet case is an artifact of LO QCD which constrains the W to balance the p_T of the jet, required to exceed 30 GeV.) The insensitivity of the polarization fractions to the number of jets holds just as well at NLO. Another interesting feature is the insensitivity of the W polarization to the jet cuts for $p_T^W > 50$ GeV. This feature is illustrated in Fig. 8 for $W^+ + 2$ -jet

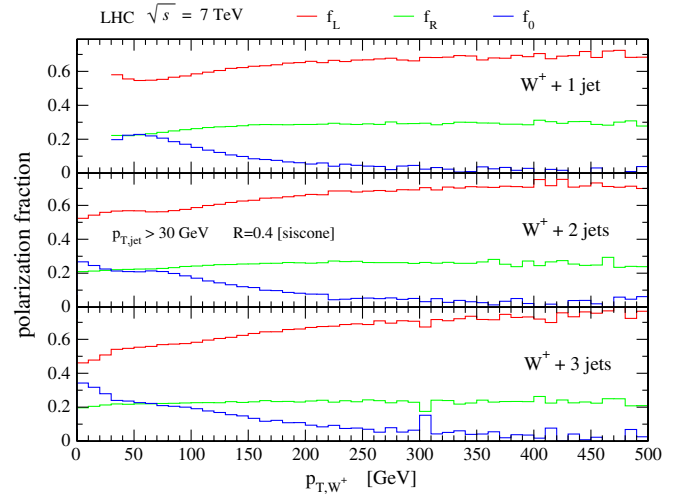


FIG. 7 (color online). A comparison of the polarization fractions for $W^+ + 1, 2, 3$ -jet production at LO, illustrating the insensitivity of the polarization fractions to the number of jets. The top panel shows the polarization fractions for $W^+ + 1$ -jet production, the middle panel $W^+ + 2$ -jet production, and the third panel $W^+ + 3$ -jet production. In each panel (except at low p_T^W) the top curve (red) gives f_L , the middle curve (green), f_R , and the bottom one (blue), f_0 .

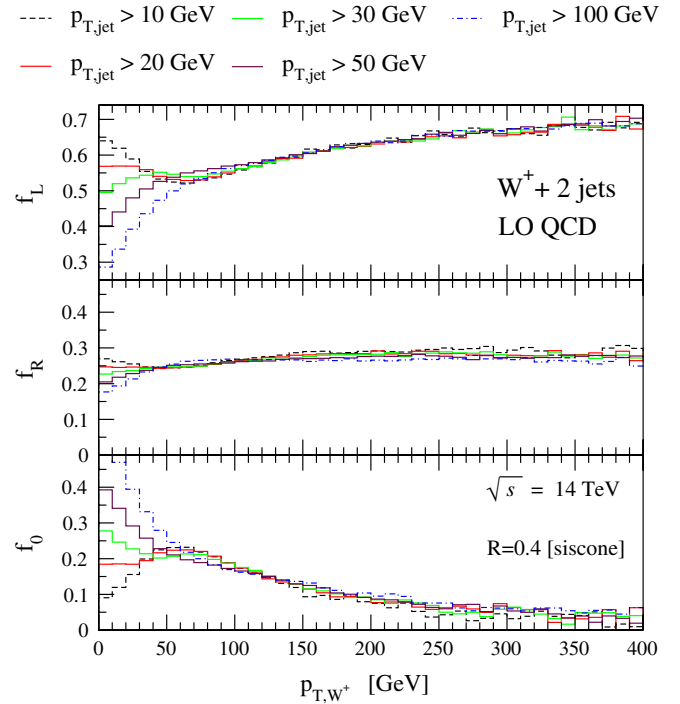


FIG. 8 (color online). The polarization fractions in $W + 2$ -jet production as a function of p_T^W , with jet cuts of $p_{T,jet} > 10, 20, 30, 50, 100$ GeV, at LO. The dashed (black) curve corresponds to a 10 GeV cut and the dot-dashed (blue) curve corresponds to a 100 GeV cut; the others are in between. At small p_T^W the 10 GeV cut gives the largest f_L and f_R fractions, while the 100 GeV cut gives the smallest f_L and f_R fractions. Above $p_T^W = 50$ GeV there is little sensitivity to the jet cuts. The center-of-mass energy is $\sqrt{s} = 14$ TeV.

production, varying jet cuts from 10 to 100 GeV. The setup in this illustration is the same as for Fig. 7, except the pp center-of-mass energy is $\sqrt{s} = 14$ TeV, instead of $\sqrt{s} = 7$ TeV. The insensitivity to the number of jets, and to the jet cuts, also holds for W^- production.

Interestingly, Z bosons behave similarly at the LHC, achieving a slightly lower polarization but with f_L still reaching above 60%, as shown in Fig. 9. This lowering happens because Z bosons do couple to right-handed quarks, and right-handed initial-state quarks lead to reversed vector-boson polarization. (The u quarks producing Z bosons are 16% right handed, 84% left handed, while the d quarks are only 3% right handed, for $\sin^2\theta_W = 0.23$.) However, the Z polarization is more difficult to measure because it is less efficiently analyzed by $Z \rightarrow l^+l^-$, as the Z coupling to the leptons is close to equally left and right handed. The analyzing power is only about 15% in the leptonic Z decay, versus 100% for $W \rightarrow l\nu$.

The analysis of high- p_T W production at the Tevatron differs because it is a $p\bar{p}$ collider. Here the weighting of the partonic subprocesses represented in Figs. 4–6 is quite different, with Fig. 5 ($u\bar{d} \rightarrow W^+g$) much more important, because both incoming quarks are now valence quarks. Because this subprocess does not lead to a large net left-handed W polarization and because the $ug \rightarrow W^+d$ and $g\bar{d} \rightarrow W^+\bar{u}$ subprocesses are quite close in magnitude (and lead to opposite left vs right polarization), we expect $f_L \approx f_R$ for both W^+ and W^- . The CP invariance of the initial state implies that $f_L(W^\pm) = f_R(W^\mp)$, neglecting CP violation, and as long as the acceptances are symmetric with respect to reversing the p and \bar{p} directions. However, one can increase the polarization of W^+ bosons with nonvanishing p_T at the Tevatron by requiring them to be in the forward hemisphere (the proton direction). Such a cut will increase the contribution of $ug \rightarrow W^+d$ relative to $g\bar{d} \rightarrow W^+\bar{u}$.

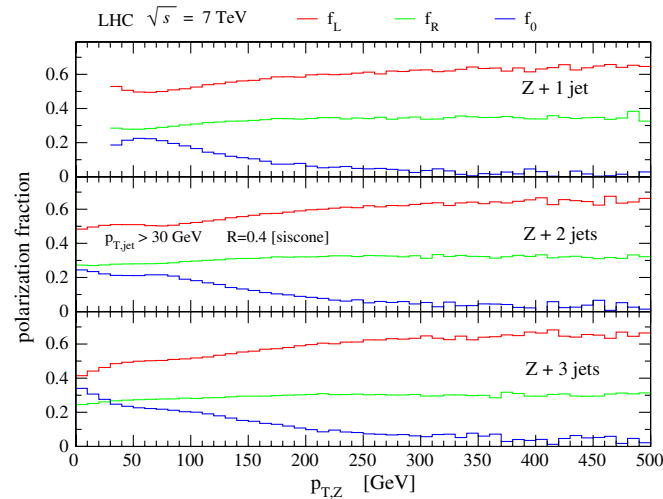


FIG. 9 (color online). The same comparison as in Fig. 7, except for Z bosons.

III. DEFINING AND COMPUTING POLARIZATION

A. Polar-angle dependence

The angular distribution of the leptonic W decay products in the W rest frame is given by a standard helicity analysis, predicated on the spin-1 nature of the W and the fact that the fermions (antifermions) to which it decays are purely left handed (right handed). First, we consider the distribution in the polar angle θ^* , after integrating over the azimuthal angle ϕ^* . We boost from the lab frame to the W rest frame. In this frame, we define θ^* to be the angle between the W flight direction, as observed in the lab frame, and the charged lepton. This angle takes values in the interval $[0, \pi]$. The distribution in θ^* , in terms of the polarization fractions f_L , f_R , and f_0 , is [2]

$$\frac{1}{\sigma} \frac{d\sigma}{d\cos\theta^*} = \frac{3}{8} (1 \mp \cos\theta^*)^2 f_L + \frac{3}{8} (1 \pm \cos\theta^*)^2 f_R + \frac{3}{4} \sin^2\theta^* f_0, \quad (3.1)$$

where the upper sign is for W^+ and the lower sign for W^- . The normalizations are chosen so that

$$\int_{-1}^1 d\cos\theta^* \frac{1}{\sigma} \frac{d\sigma}{d\cos\theta^*} = f_L + f_0 + f_R = 1. \quad (3.2)$$

For a left-handed W^+ the decay amplitude must vanish at $\theta^* = 0$ because angular momentum would be violated in a decay to a forward-going right-handed antilepton and a backward-going left-handed lepton. This explains why the f_L term is proportional to $(1 - \cos\theta^*)^2$ for W^+ . Similarly, for a right-handed W^+ , the decay must vanish for $\theta^* = \pi$, explaining the factor of $(1 + \cos\theta^*)^2$ multiplying f_R . Decays of the longitudinal mode are forbidden at both $\theta^* = 0$ and $\theta^* = \pi$, explaining the $\sin^2\theta^*$ behavior. The W^- case behaves oppositely because the charged lepton is now left handed rather than right handed.

In Eq. (3.1), σ can be a differential cross section. For example, Eq. (3.1) is just as valid if we replace

$$\sigma \rightarrow \frac{d\sigma}{dp_T^W}. \quad (3.3)$$

In fact, any differential cross section that does not depend on the kinematics of individual leptons can be used. Inserting such a distribution into Eq. (3.1) allows us to define polarization fractions f_L , f_R , and f_0 as a function of the W boson kinematics, number of jets, and so forth.

We can define the expectation of an observable $g(\theta^*)$ via

$$\langle g(\theta^*) \rangle \equiv \int_{-1}^1 g(\theta^*) \frac{1}{\sigma} \frac{d\sigma}{d\cos\theta^*} d\cos\theta^*. \quad (3.4)$$

In particular, the expectation value $\langle \cos\theta^* \rangle$ is

$$\begin{aligned} \langle \cos\theta^* \rangle &= \int_{-1}^1 \cos\theta^* \frac{1}{\sigma} \frac{d\sigma}{d\cos\theta^*} d\cos\theta^* = \mp \frac{1}{2} (f_L - f_R) \\ &= \pm \left(\frac{1}{2} - f_L - \frac{1}{2} f_0 \right). \end{aligned} \quad (3.5)$$

We can obtain other moments similarly, such as

$$\langle \cos^2 \theta^* \rangle = \frac{2}{5} - \frac{1}{5} f_0, \quad (3.6)$$

$$\langle \cos^4 \theta^* \rangle = \frac{9}{35} - \frac{6}{35} f_0. \quad (3.7)$$

Solving for the longitudinal fraction f_0 gives

$$f_0 = 2 - 5 \langle \cos^2 \theta^* \rangle, \quad (3.8)$$

or

$$f_0 = \frac{3}{2} - \frac{35}{6} \langle \cos^4 \theta^* \rangle. \quad (3.9)$$

We compute lepton decay distributions numerically by Monte Carlo sampling, and we accumulate several different moments at once. Using the two formulas (3.8) and (3.9) should give the same answer for f_0 .

Finally, by plugging in Eq. (3.8) into Eq. (3.5) we can solve for the left- and right-handed polarization fractions,

$$\begin{aligned} f_L &= -\frac{1}{2} \mp \langle \cos \theta^* \rangle + \frac{5}{2} \langle \cos^2 \theta^* \rangle, \\ f_R &= -\frac{1}{2} \pm \langle \cos \theta^* \rangle + \frac{5}{2} \langle \cos^2 \theta^* \rangle, \end{aligned} \quad (3.10)$$

where again the top sign is for W^+ and the bottom sign is for W^- .

B. Inclusion of the azimuthal angle

As mentioned in Sec. I, detector effects such as finite resolution, acceptance, and reconstruction efficiency distort angular distributions, so that the extracted polarization fractions are sensitive to how the cross section depends on the azimuthal angle ϕ^* as well as θ^* . We therefore give the complete dependence of the cross section on θ^* and ϕ^* . Similar angular decompositions may be found in Refs. [13–18]. One important difference is that we do not use the Collins-Soper frame [13] but rather define angles using the W boson flight direction. As we saw in the previous section, this definition reveals the left-handed nature of the produced W bosons quite cleanly.

As before, we boost from the lab frame to the W rest frame. The W flight direction defines the z axis. The (x, y) plane is orthogonal to the z axis, and (x, y, z) form a right-handed coordinate system (see Fig. 10). The azimuthal angle ϕ^* takes values in $[0, 2\pi)$ and is equal to 0 in the positive x direction, $\pi/2$ in the positive y direction. The x axis is defined by the intersection of the plane spanned by the two proton momenta with the (x, y) plane. Finally, the orientation of the positive x axis is defined using the proton momenta. The positive x axis is defined [12] to point in the direction of the proton with the smaller angular separation from the z axis (P_2 in the case shown in Fig. 10).

We consider the decay distribution of the W boson at finite p_T^W in terms of the lepton angles defined in Fig. 10.

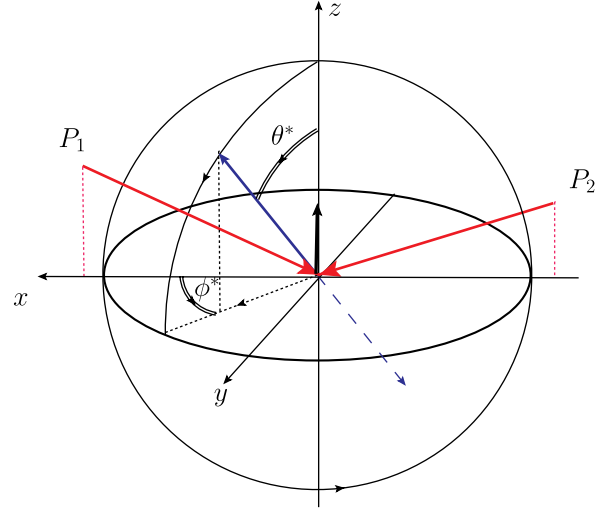


FIG. 10 (color online). The lepton decay angles in the W rest frame. The original W flight direction, defining the z axis, is represented by a dark (black) arrow. The protons, represented by angled (red) arrows pointing at the origin, lie in the (x, z) plane. The momenta of the charged lepton and the neutrino are given by the solid and dashed blue arrows, respectively. The decay angle θ^* is measured with respect to the z axis. The origin of the azimuthal angle ϕ^* is along the x axis, which lies in the plane defined by the proton momenta. The positive x axis points in the direction of motion of the proton with the smaller angular separation from the z axis (P_2 here). The coordinate system is right handed, which defines the direction of the y axis.

Following Refs. [13–18], we decompose the cross section as

$$\begin{aligned} & \frac{1}{\sigma} \frac{d\sigma}{d(\cos\theta^*)d\phi^*} \\ &= \frac{3}{16\pi} \left[(1 + \cos^2\theta^*) + A_0 \frac{1}{2} (1 - 3\cos^2\theta^*) \right. \\ & \quad + A_1 \sin 2\theta^* \cos\phi^* + A_2 \frac{1}{2} \sin^2\theta^* \cos 2\phi^* \\ & \quad + A_3 \sin\theta^* \cos\phi^* + A_4 \cos\theta^* + A_5 \sin\theta^* \sin\phi^* \\ & \quad \left. + A_6 \sin 2\theta^* \sin\phi^* + A_7 \sin^2\theta^* \sin 2\phi^* \right]. \end{aligned} \quad (3.11)$$

Here we define the expectation value as

$$\begin{aligned} \langle f(\theta^*, \phi^*) \rangle &= \int_{-1}^1 d(\cos\theta^*) \int_0^{2\pi} d\phi^* \frac{1}{\sigma} \\ & \quad \times \frac{d\sigma}{d(\cos\theta^*)d\phi^*} f(\theta^*, \phi^*). \end{aligned} \quad (3.12)$$

As before, σ can be any differential cross section that does not depend on the individual lepton kinematics.

Following similar logic as for the previous case, in which the azimuthal angle has been integrated out, we may extract the angular coefficients A_i directly in terms of expectation values,

$$\begin{aligned}
A_0 &= 4 - 10 \langle \cos^2 \theta^* \rangle, & A_1 &= \langle 5 \sin 2\theta^* \cos \phi^* \rangle, \\
A_2 &= \langle 10 \sin^2 \theta^* \cos 2\phi^* \rangle, & A_3 &= \langle 4 \sin \theta^* \cos \phi^* \rangle, \\
A_4 &= \langle 4 \cos \theta^* \rangle, & A_5 &= \langle 4 \sin \theta^* \sin \phi^* \rangle, \\
A_6 &= \langle 5 \sin 2\theta^* \sin \phi^* \rangle, & A_7 &= \langle 5 \sin^2 \theta^* \sin 2\phi^* \rangle.
\end{aligned}
\tag{3.13}$$

For either LO or ME+PS, the coefficients A_5 , A_6 , A_7 vanish because the functions they multiply are odd under a “naive” time-reversal symmetry as well as under parity, either of which maps $\phi^* \rightarrow -\phi^*$. They do receive contributions at NLO in QCD from the absorptive part of one-loop amplitudes [15,18]. However, the p_T^W distribution of these contributions is highly suppressed at the LHC. The left panel of Fig. 11 shows that the A_5 coefficient is well below 0.01, and indeed is consistent with zero, within integration errors due to sampling fluctuations. However, from the right panel of Fig. 11, we see that this suppression is simply due to a cancellation between the forward and backward regions in rapidity. The rapidity distributions for A_6 and A_7 are smaller than the one for A_5 . An analogous computation for the parity-odd coefficients, both in $p\bar{p}$ and pp collisions up to 20 TeV, was given in Ref. [15] but using the Collins-Soper frame. Similar results hold when the W^+ is replaced by a W^- . In the remaining part of this paper, we will not distinguish between the forward and backward rapidity regions, and we will not discuss A_5 , A_6 , and A_7 further.

If we integrate the combined distribution in θ^* and ϕ^* , Eq. (3.11), over the azimuthal angle ϕ^* , we should recover Eq. (3.1) for the polar-angle distribution. Carrying out the integration, we obtain

$$\begin{aligned}
&\frac{1}{\sigma} \frac{d\sigma}{d(\cos\theta^*)} \\
&= \frac{3}{8} \left[(1 + \cos^2\theta^*) + A_0 \frac{1}{2} (1 - 3\cos^2\theta^*) + A_4 \cos\theta^* \right].
\end{aligned}
\tag{3.14}$$

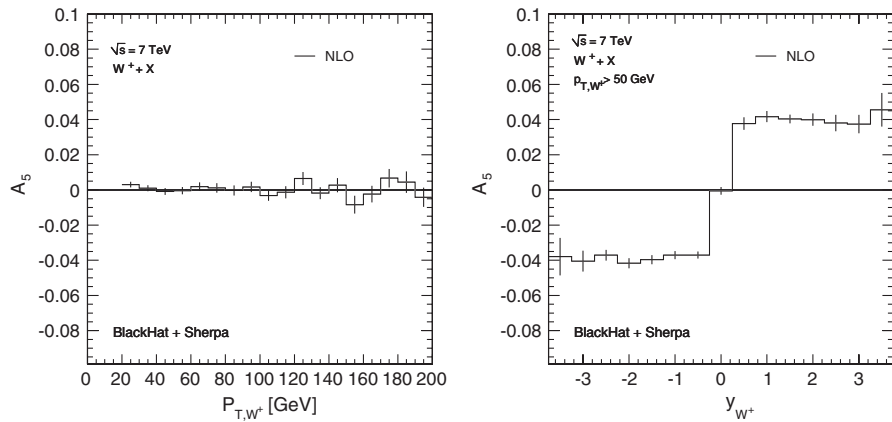


FIG. 11. The left panel shows A_5 as a function of p_T^W for W^+ with any number of jets at the LHC at NLO; the result is very small, if not vanishing. The right panel shows A_5 as a function of the rapidity, with a cut of $p_T^W > 50$ GeV imposed. The thin vertical lines give the integration errors.

Comparing to Eq. (3.1), we see that the polarization fractions are given in terms of the A_i as

$$f_L = \frac{1}{4}(2 - A_0 \mp A_4), \quad f_R = \frac{1}{4}(2 - A_0 \pm A_4), \quad f_0 = \frac{1}{2}A_0,
\tag{3.15}$$

with the top sign for W^+ , the bottom sign for W^- . We also have $f_L - f_R = \mp A_4/2$.

IV. RESULTS

In this section we present our results for the polarization coefficients. Prior to presenting them, we summarize our calculational setup based on BLACKHAT [20] and SHERPA [21]. We will present results for both NLO parton-level QCD and the ME+PS framework. For reference, to gauge the size of higher-order QCD corrections, we also present results at LO fixed-order parton-level. We find that the polarization fractions are quite insensitive to variations of a common renormalization and factorization scale, so varying the scale does not offer a reasonable estimate of the theoretical uncertainty. Instead, we use the difference between the NLO and ME+PS predictions as a measure of the uncertainty. The two frameworks have competing strengths. The NLO result benefits from true virtual corrections and a better cancellation of scale dependence in the overall cross section. The ME+PS result includes the effects of radiating multiple soft gluons. The similarity of both predictions gives us confidence that further refinement in the order (fixed or logarithmic) perturbative expansion will not lead to large changes in these observables.

A. Setup

We use SHERPA for several different purposes: computing the basic fixed-order LO predictions, generating the ME+PS predictions, and providing the phase-space integration framework as well as the real-emission contributions to the fixed-order NLO predictions. ME+PS event samples are produced according to the technique described

in Ref. [25]. This method combines two essentially different approaches to perturbative QCD, hard matrix-element calculations, which are exact at some fixed perturbative order (LO in our case), and parton showers, which resum logarithmic corrections due to Bremsstrahlung effects. The parton shower employed to this end in SHERPA [26] is based on Catani-Seymour dipole factorization [27]. In contrast to earlier parton showers, the model inherently respects QCD soft color coherence, as the eikonal factors associated with soft-gluon emission off a color dipole are exactly mapped onto two dipole functions, which differ only in the assignment of emitter and spectator partons. Additionally, the model allows the unambiguous identification of a recoil partner for partons that are shifted off mass shell in the splitting process (the “mother” partons), thereby eliminating one of the major sources of uncertainty in earlier schemes for parton evolution. As the observables presented below should be insensitive to hadronization effects, ME+PS results are presented at the parton level. We match to matrix elements containing up to three final-state partons and use 15 GeV for the merging cut. For the ME+PS calculations we use the MSTW08 NLO parton distributions [28]. An identical simulation, but using the MSTW08 LO set, gives very similar results, except for the total cross section of the event sample.

To obtain the NLO results we use BLACKHAT in conjunction with SHERPA. We use the same basic setup employing on-shell methods, as in earlier computations of $W + 3$, 4-jet and $Z, \gamma^* + 3$ -jet production [1,6,8]. For W production with two or fewer tagged jets, BLACKHAT uses analytic formulas for the virtual contributions [29]. For $W + 3$ -jet production (as in Fig. 1) BLACKHAT evaluates these contributions numerically. The remaining NLO ingredients, the real-emission and dipole-subtraction terms [27], are computed by AMEGIC++ [4], part of the SHERPA package [21]. We also use SHERPA to perform phase-space integration using QCD antenna structures [30].

In all cases, we include the full W Breit-Wigner resonance and decays to leptons retain all spin correlations. Except where noted, for our NLO calculations we use the MSTW08 NLO parton distribution functions [28]. For LO we use the MSTW08 LO set. Following Refs. [8,9], we use half the partonic total transverse energy, $\hat{H}'_T/2$ as our reference renormalization- and factorization-scale choice for LO and NLO. (We define $\hat{H}'_T \equiv \sum_j p_T^j + E_T^W$, where the

sum runs over all final-state partons j and $E_T^W \equiv \sqrt{M_W^2 + (p_T^W)^2}$. The W transverse energy E_T^W is used, instead of the lepton sum $E_T^l + E_T^{\nu}$, to prevent the scale choice from biasing the leptonic angular variables.) We found very similar NLO results using a second, Catani-Krauss-Kuhn-Webber-style scale choice [5]. The standard-model parameters are the same as in Ref. [1], except the value of α_s is set to that employed by MSTW08.

We used SHERPA version 1.3.0 [31]. The virtual matrix elements we employed are available in Ref. [29], except for the $W + 3$ -jet matrix elements used in Fig. 1, which are computed numerically by BLACKHAT.

B. Polarization predictions

In Table I we give our predictions for the polarization fractions f_L, f_R , and f_0 at the LHC for both W^+ and W^- . The W bosons are required to have $p_T^W > 50$ GeV, but there is no cut on their rapidity, and no explicit jet requirements are imposed. We show predictions using NLO, ME+PS, and LO. The LO prediction is the least reliable of the three and is given only for reference purposes, to show the effect of higher-order QCD corrections. This table makes clear that *both* W^+ and W^- bosons are predominantly left handed. Because the polarization fractions are normalized by the cross section, and because we treat the scale dependence in a correlated fashion, the renormalization- and factorization-scale dependence is very small, under 2% at NLO for all fractions. It is even smaller at LO, but only because the running of the coupling completely drops out from the polarization fractions. A more sensible estimate of the theoretical uncertainty is the difference between NLO and ME+PS. Table I shows that this difference is under 10% for the polarization fractions.

Our results for the A_i asymmetry coefficients of Eq. (3.11) are shown in Table II. Again taking the difference between the NLO and ME+PS results as an estimate of the theoretical uncertainty, we see that the uncertainty is under 10%, except for A_4 , in which it is about 10%, and A_3 , which is very small but has a large percentage shift between NLO and ME+PS. As mentioned previously, the A_5, A_6 , and A_7 coefficients vanish at LO and for ME+PS. At NLO, they are much smaller than the current experimental and theoretical uncertainties and can therefore be neglected.

CMS recently presented a measurement of the polarization fractions [12]. In Table III we compare our theoretical

TABLE I. The polarization fractions for W production with $p_T^W > 50$ GeV and no restrictions on either the W rapidity or the number of associated jets. The numbers in parentheses indicate the numerical integration error in the last digit; if no integration error is indicated this error is smaller than the roundoff error.

	W^+ NLO	W^+ ME+PS	W^+ LO	W^- NLO	W^- ME+PS	W^- LO
f_L	0.555(1)	0.548(1)	0.556	0.527(1)	0.521(1)	0.522
f_R	0.247(1)	0.265(1)	0.247	0.280(1)	0.300(1)	0.288
f_0	0.199(1)	0.187(1)	0.197	0.193(1)	0.179(1)	0.190

TABLE II. The A_i coefficients for W production with $p_T^W > 50$ GeV and no restrictions on either the W rapidity or the number of associated jets.

	W^+ NLO	W^+ ME+PS	W^+ LO	W^- NLO	W^- ME+PS	W^- LO
A_0	0.397(1)	0.375(2)	0.395	0.387(1)	0.358(2)	0.379
A_1	-0.114(1)	-0.106(2)	-0.135	-0.111(1)	-0.107(1)	-0.131
A_2	0.322(2)	0.337(3)	0.394(1)	0.315(2)	0.327(3)	0.379
A_3	-0.014(1)	-0.055(1)	-0.015	0.000(1)	0.031(1)	0.000
A_4	-0.616(1)	-0.565(2)	-0.619	0.495(1)	0.443(2)	0.468

TABLE III. A comparison of theoretical predictions for $f_L - f_R$ and f_0 to preliminary CMS results [12]. The first uncertainty in the CMS measurement is statistical, and the second is systematic.

	CMS	NLO	ME+PS	LO
$W^+(f_L - f_R)$	$0.300 \pm 0.031 \pm 0.034$	0.308	0.283	0.309
$W^-(f_L - f_R)$	$0.226 \pm 0.031 \pm 0.050$	0.248	0.222	0.234
$W^+ f_0$	$0.192 \pm 0.075 \pm 0.089$	0.199	0.187	0.197
$W^- f_0$	$0.162 \pm 0.078 \pm 0.136$	0.193	0.179	0.190

predictions for $(f_L - f_R)$ and f_0 to the experimental ones. Various corrections for effects such as acceptance cuts have been applied by CMS in order to produce the numbers in the table. The NLO or ME+PS predictions are both in excellent agreement with the data, within the experimental uncertainties. Large increases in the LHC data sets are anticipated in the near future. The improvement in experimental precision that can be expected with these data should provide even more incisive tests, possibly differentiating between the NLO and ME+PS predictions.

Figure 12 shows the $\cos\theta^*$ distributions for both W^+ and W^- bosons with $p_T^W > 50$ GeV. These plots show that in

the W^+ case, the charged antilepton prefers to go backward with respect to the W flight direction, while in the W^- case the charged lepton tends to go forward, in accordance with the left-handed polarizations given in Table I.

Figure 13 displays the polarization fraction f_L for both W^+ and W^- bosons at the LHC, as a function of the vector bosons' transverse momenta. There are again no rapidity cuts and no explicit jet requirements (in contrast to the setup for Figs. 7 and 9). The fraction f_L climbs to around 0.7 at high p_T^W . The NLO predictions are a bit higher than the LO and ME+PS ones. Figure 14 contains the corresponding plots for the right-handed fraction f_R . Although this component rises initially, by 150 GeV it stabilizes between 0.25 to 0.30 for the W^+ case. For the W^- case, it is a bit higher. For f_R the NLO predictions are a bit lower than the LO and ME+PS ones. In any case, to compensate for these rises, the longitudinal component f_0 falls rapidly with increasing p_T^W , as illustrated in Fig. 15. As mentioned previously, the decline of f_0 is due to the equivalence theorem. A rather striking feature of these plots is how small the difference is between the W^- and W^+ cases, showing that the effect is essentially the same for both signs.

Another interesting plot is the left-handed polarization fraction f_L as a function of p_T^W but with different rapidity

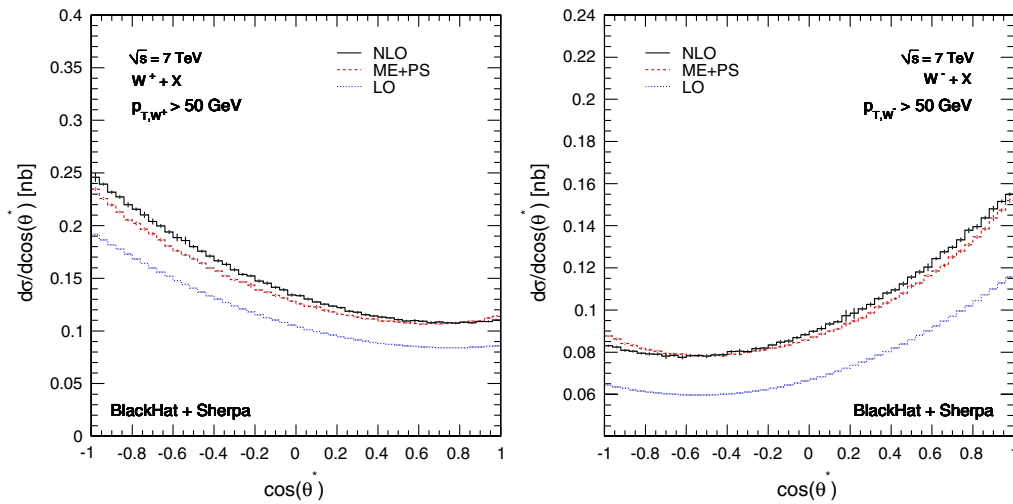


FIG. 12 (color online). The $\cos\theta^*$ distribution of the charged leptons for W^\pm production with $p_T^W > 50$ GeV. The left plot shows the distribution in W^+ production and the right plot, that in W^- production. Three different results are shown: the fixed-order NLO result represented by the solid (black) line, the ME+PS result represented by the dashed (red) line, and the fixed-order LO result represented by the dotted (blue) line. The thin vertical lines indicate the integration errors.

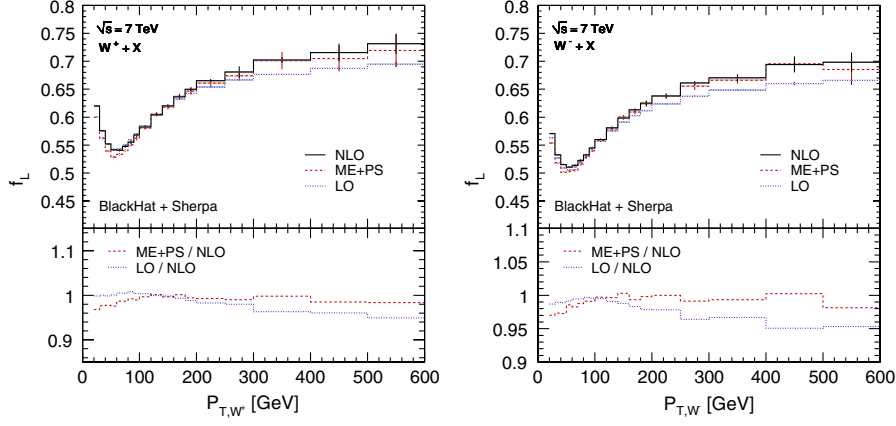


FIG. 13 (color online). The left-handed polarization fraction f_L as a function of p_T^W for W^\pm production at the LHC. The left panel gives the W^+ case and the right panel the W^- case. Three different results are shown: the fixed-order NLO result represented by the solid (black) line, the ME+PS result represented by the dashed (red) line, and the fixed-order LO result represented by the dotted (blue) line. The thin vertical lines indicate the integration errors. The lower panels show ratios normalized to the NLO result.

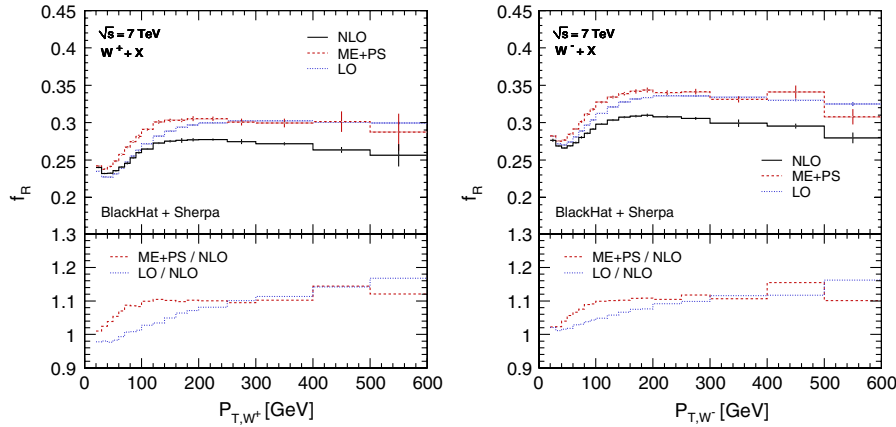


FIG. 14 (color online). The coefficient f_R as a function of p_T^W . The left panel is for W^+ and the right panel for W^- . The format is the same as in Fig. 13.

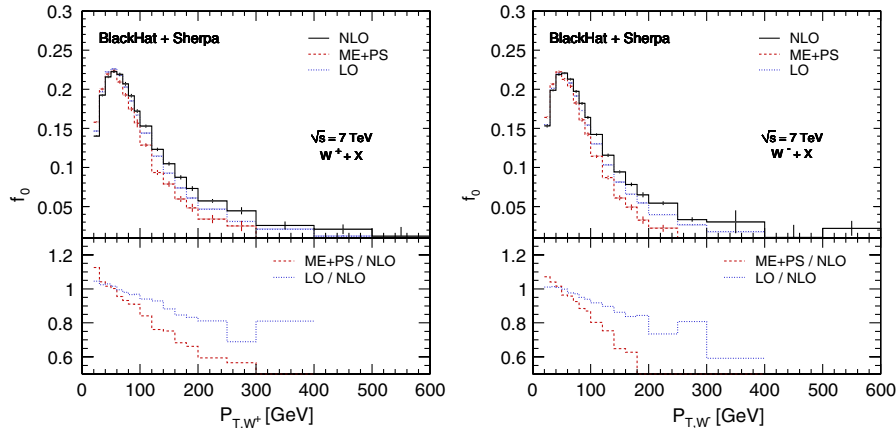


FIG. 15 (color online). The coefficient $f_0 = A_0/2$ as a function of p_T^W . It vanishes at large p_T^W by the equivalence theorem. The left panel is for W^+ and the right panel for W^- . The format is the same as in Fig. 13.

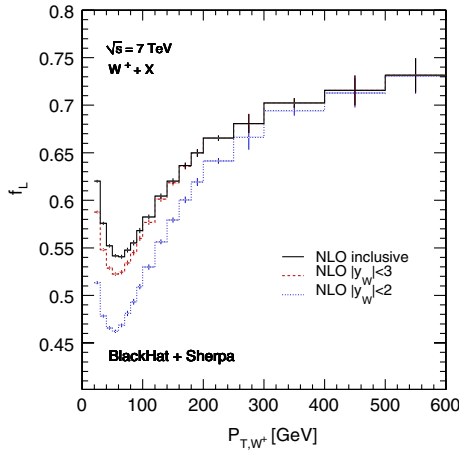


FIG. 16 (color online). The f_L polarization fraction in NLO QCD for the W^+ case. The solid (black) curve shows the fraction with no rapidity cut, the dashed (red) curve with a cut $|y_W| < 2$, and the dotted (blue) curve with $|y_W| < 3$. (The vertical axis starts at $f_L = 0.4$ to visually separate the curves.)

cuts imposed on the vector boson y_W . In Fig. 16 we show the three curves, one with no rapidity cut, one with $|y_W| < 2$, and one with $|y_W| < 3$. At low p_T^W , the polarization fraction in the central region with $|y_W| < 2$ is lower than for $|y_W| < 3$, which in turn is lower than the fraction with no rapidity cut imposed. At low p_T , f_L picks up a large left-handed polarization in the forward and backward regions from the beam-axis effect described in Sec. II, while the transverse effect has not fully kicked in. By a transverse momentum of 150 GeV, the effect of the $|y_W| < 3$ cut has essentially disappeared; and by a transverse momentum of 350 GeV, the effect of any rapidity cut has essentially disappeared. This demonstrates that the large polarization at high p_T^W comes from central rapidities. One could impose a rapidity cut on the W boson in order to separate the beam-axis polarization effect from the transverse one at all vector-boson transverse momenta.

Finally in Fig. 17, we compare the five A_i coefficients for the cases of W^+ and W^- using NLO QCD. Up to sign flips for A_3 and A_4 we see little difference between the two cases, as a function of p_T^W . The approximate equality $A_0 \approx A_2$ is due to the (frame-independent) Lam-Tung relation [14], which holds at LO, but is violated at NLO.

V. CONCLUSIONS

Prompt W vector bosons of both signs, when produced at moderate to high transverse momentum at the LHC, are predominantly polarized left handedly [1,10]. In this paper, we presented a detailed study of this phenomenon and of its underlying mechanism. The effect, which superficially appears to violate CP, actually arises from a combination of the left-handed nature of the electroweak charged-current interaction, the prevalence of valence quarks in the pp initial state (which is not charge-conjugation invariant), and properties of the short-distance matrix elements.

We found that a simple estimate, assuming 90° scattering in the partonic center-of-mass for the dominant process $qg \rightarrow Wq'$, leads to 80% left-handed polarization for W bosons at large p_T^W . This high degree of polarization is somewhat reduced by kinematic effects in this subprocess, as well as dilution from other subprocesses, especially at lower p_T^W . Nevertheless, with a cut of $p_T^W > 50$ GeV we find that most W bosons are left handed, and the remainder are split between right-handed and longitudinal states. As p_T^W increases, the left-handed polarization fraction can rise as high as 70%. This is remarkably close to the simple upper estimate of 80%. The Z boson polarization is similar, though a bit smaller at around 60%, due to dilution from right-handed u quarks in the initial state. The effect in Z decays will be harder to see experimentally, however, as the analyzing power in decays to charged leptons is only about 15% (versus 100% for $W \rightarrow l\nu$).

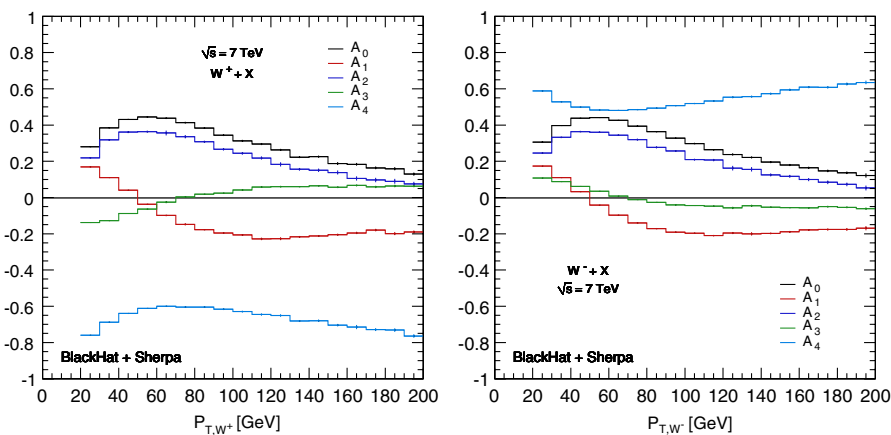


FIG. 17 (color online). The first five A_i as a function of p_T^W at NLO. The left panel is for W^+ production and the right panel for W^- production. Starting from the top and proceeding downwards, the left-hand sides of the curves at low p_T^W are in the order A_0, A_2, A_1, A_3, A_4 for the left panel. For the right panel they are in the order A_4, A_0, A_2, A_1, A_3 .

We studied the polarization dominance using LO, NLO, and ME+PS QCD calculations. The effect is theoretically robust, and higher-order QCD corrections are small. The difference between NLO and ME+PS predictions suggests a 10% theoretical uncertainty in the polarization fractions. It should be possible in the future to improve the predictions, when there are no tagged jets, or even one tagged jet, in at least two ways. First, it should be possible to generate $W + 1$ -jet events at NLO accuracy incorporating a parton shower, as a program already exists for the closely-related case of $Z + 1$ -jet production [32] based on the POWHEG method [33]. The MC@NLO approach [34] should also be feasible. Second, the computation of $W + 1$ -jet production at NNLO in QCD may become feasible before long [35], making it possible to study the polarization observables at one higher order in α_s .

We provided numerical tables and plots for the polarization fractions and compared to the recent preliminary measurement by the CMS Collaboration [12]. The theoretical predictions are in excellent agreement with this initial measurement, given its relatively sizable uncertainties. More detailed comparisons will be possible with increased data sets from the ongoing run of the LHC.

It may also be possible to use the W polarization phenomenon as a probe of polarized gluon distribution functions, if a sufficient number of W bosons can be produced at moderate transverse momentum in polarized proton collisions. Asymmetries in inclusive (low p_T^W) W boson production in polarized pp collisions have recently been studied at the Relativistic Heavy Ion Collider [36].

The large left-handed polarization of prompt vector bosons at high-transverse momentum is a robust theoretical prediction, stable against both QCD corrections and the emission of additional jets. It leads to very different distributions for the positively and negatively charged decay leptons, as well as for the neutrinos. The situation for top-quark pair production is very different. The initial state

is predominantly all gluon, and hence CP invariant, so no such asymmetry is possible. While top-quark decay produces W^+ bosons that are about 70% longitudinal, 30% left handed, the W^- bosons from \bar{t} decay are 70% longitudinal, 30% right handed, so in this case the positively and negatively charged leptons have very similar distributions. The decay to WW pairs of a heavy Higgs boson (sufficiently heavy to decay to moderately high- p_T W bosons) is another signal process which should not display single- W asymmetries because of the spin-0 nature of the Higgs boson. The same will hold true for W bosons arising from many sources beyond standard-model physics. These distinctions give W polarization the potential to be a powerful discriminant for interesting standard-model signals and new physics beyond the standard model.

ACKNOWLEDGMENTS

We thank Carola Berger for contributions at the initial stages of this project. We are grateful to Oliver Buchmüller, Jad Marrouche, Roberto Peccei, Michael Peskin, Jeff Richman, David Saltzberg, Paris Sphicas, and Markus Stoye for useful conversations. This research was supported by the US Department of Energy under Contracts Nos. DE-FG03-91ER40662 and DE-AC02-76SF00515. D.A.K.'s research is supported by the European Research Council under Advanced Investigator Grant No. ERC-AdG-228301. H.I.'s and S.H.'s work are supported by a grant from the US LHC Theory Initiative through NSF Contract No. PHY-0705682. This research used resources of Academic Technology Services at UCLA, PhenoGrid using the GridPP infrastructure.

Note added.—After the first version of this article appeared, CMS [37] has produced a paper on the W polarization measurement at the LHC; also, CDF [38] has measured several A_i coefficients for Z production with transverse momentum at the Tevatron, using the Collins-Soper frame.

-
- [1] C. F. Berger *et al.*, *Phys. Rev. D* **80**, 074036 (2009).
 - [2] R. K. Ellis, W. J. Stirling, and B. R. Webber, *QCD and Collider Physics* (Cambridge University Press, Cambridge, England, 1996).
 - [3] T. Stelzer and W. F. Long, *Comput. Phys. Commun.* **81**, 357 (1994); A. Pukhov *et al.*, [arXiv:hep-ph/9908288](https://arxiv.org/abs/hep-ph/9908288); M. L. Mangano, M. Moretti, F. Piccinini, R. Pittau, and A. D. Polosa, *J. High Energy Phys.* **07** (2003) 001.
 - [4] F. Krauss, R. Kuhn, and G. Soff, *J. High Energy Phys.* **02** (2002) 044; T. Gleisberg and F. Krauss, *Eur. Phys. J. C* **53**, 501 (2007).
 - [5] S. Catani, F. Krauss, R. Kuhn, and B. R. Webber, *J. High Energy Phys.* **11** (2001) 063; M. Mangano, M. Moretti, F. Piccinini, and M. Trecanni, *J. High Energy Phys.* **01** (2007) 013.
 - [6] C. F. Berger *et al.*, *Phys. Rev. Lett.* **102**, 222001 (2009).
 - [7] R. K. Ellis, K. Melnikov, and G. Zanderighi, *Phys. Rev. D* **80**, 094002 (2009); K. Melnikov and G. Zanderighi, *Phys. Rev. D* **81**, 074025 (2010).
 - [8] C. F. Berger *et al.*, *Phys. Rev. D* **82**, 074002 (2010).
 - [9] C. F. Berger *et al.*, *Phys. Rev. Lett.* **106**, 092001 (2011).
 - [10] C. F. Berger *et al.*, Proc. Sci., RADCOR2009 (2009) 002.
 - [11] J. M. Cornwall, D. N. Levin, and G. Tiktopoulos, *Phys. Rev. D* **10**, 1145 (1974); **11**, 972(E) (1975).
 - [12] P. Harris (CMS Collaboration), *Rencontres de Moriond EW 2011* La Thuile, Italy, (2011).

- [13] J.C. Collins and D.E. Soper, *Phys. Rev. D* **16**, 2219 (1977).
- [14] C.S. Lam and W.-K. Tung, *Phys. Rev. D* **21**, 2712 (1980).
- [15] K. Hagiwara, K. Hikasa, and N. Kai, *Phys. Rev. Lett.* **52**, 1076 (1984).
- [16] E. Mirkes, *Nucl. Phys. B* **387**, 3 (1992).
- [17] E. Mirkes and J. Ohnemus, *Phys. Rev. D* **50**, 5692 (1994); E. Mirkes and J. Ohnemus, *Phys. Rev. D* **51**, 4891 (1995).
- [18] K. Hagiwara, K. Hikasa, and H. Yokoya, *Phys. Rev. Lett.* **97**, 221802 (2006).
- [19] D.E. Acosta *et al.* (CDF Collaboration), *Phys. Rev. D* **73**, 052002 (2006).
- [20] C.F. Berger *et al.*, *Phys. Rev. D* **78**, 036003 (2008).
- [21] T. Gleisberg *et al.*, *J. High Energy Phys.* **02** (2004) 056; T. Gleisberg *et al.*, *J. High Energy Phys.* **02** (2009) 007.
- [22] J. Pumplin *et al.*, *J. High Energy Phys.* **07** (2002) 012.
- [23] C.H. Kom and W.J. Stirling, *Eur. Phys. J. C* **69**, 67 (2010); **71**, 1546 (2011).
- [24] G.P. Salam and G. Soyez, *J. High Energy Phys.* **05** (2007) 086.
- [25] S. Höche, F. Krauss, S. Schumann, and F. Siegert, *J. High Energy Phys.* **05** (2009) 053.
- [26] S. Schumann and F. Krauss, *J. High Energy Phys.* **03** (2008) 038; S. Höche, S. Schumann, and F. Siegert, *Phys. Rev. D* **81**, 034026 (2010).
- [27] S. Catani and M.H. Seymour, *Nucl. Phys. B* **485**, 291 (1997); **510**, 503(E) (1998).
- [28] A.D. Martin, W.J. Stirling, R.S. Thorne, and G. Watt, *Eur. Phys. J. C* **63**, 189 (2009).
- [29] Z. Bern, L.J. Dixon, and D.A. Kosower, *Nucl. Phys. B* **513**, 3 (1998).
- [30] A. van Hameren and C.G. Papadopoulos, *Eur. Phys. J. C* **25**, 563 (2002); T. Gleisberg, S. Höche, and F. Krauss, [arXiv:0808.3672](https://arxiv.org/abs/0808.3672).
- [31] <http://www.hepforge.org/sherpa/>.
- [32] S. Alioli, P. Nason, C. Oleari, and E. Re, *J. High Energy Phys.* **01** (2011) 095.
- [33] S. Frixione, P. Nason, and C. Oleari, *J. High Energy Phys.* **11** (2007) 070; S. Alioli, P. Nason, C. Oleari, and E. Re, *J. High Energy Phys.* **07** (2008) 060.
- [34] S. Frixione and B.R. Webber, *J. High Energy Phys.* **06** (2002) 029; S. Frixione, P. Nason, and B.R. Webber, *J. High Energy Phys.* **08** (2003) 007.
- [35] P. Bolzoni, S. Moch, G. Somogyi, and Z. Trócsányi, *J. High Energy Phys.* **08** (2009) 079; A. Daleo, A. Gehrmann-De Ridder, T. Gehrmann, and G. Luisoni, *J. High Energy Phys.* **01** (2010) 118; *Proc. Sci., RADCOR2009* (2010) 062; *DIS2010* (2010) 122; E.W.N. Glover and J. Pires, *J. High Energy Phys.* **06** (2010) 096; *Nucl. Phys. B, Proc. Suppl.* **205–206**, 176 (2010); R. Boughezal, A. Gehrmann-De Ridder, and M. Ritzmann, *Proc. Sci., DIS2010* (2010) 101; *J. High Energy Phys.* **02** (2011) 098; P. Bolzoni, G. Somogyi, and Z. Trócsányi, *J. High Energy Phys.* **01** (2011) 059.
- [36] M.M. Aggarwal *et al.* (STAR Collaboration), *Phys. Rev. Lett.* **106**, 062002 (2011); A. Adare *et al.* (PHENIX Collaboration), *Phys. Rev. Lett.* **106**, 062001 (2011).
- [37] S. Chatrchyan *et al.* (CMS Collaboration), [arXiv:1104.3829](https://arxiv.org/abs/1104.3829).
- [38] T. Aaltonen *et al.* (CDF Collaboration), [arXiv:1103.5699](https://arxiv.org/abs/1103.5699) [*Phys. Rev. Lett.* (to be published)].